Gradient-Domain Image Reconstruction Framework with Intensity-Range and Base-Structure Constraints

Takashi Shibata[1,2], Masayuki Tanaka[1], Masatoshi Okutomi[1]
[1]Tokyo Institute of Technology, [2]NEC corporation
tshibata@ok.ctrl.titech.ac.jp, {mtanaka, mxo}@ctrl.titech.ac.jp

Abstract

This paper presents a novel unified gradient-domain image reconstruction framework with intensity-range constraint and base-structure constraint. The existing method for manipulating base structures and detailed textures are classifiable into two major approaches: i) gradient-domain and ii) layer-decomposition. To generate detail-preserving and artifact-free output images, we combine the benefits of the two approaches into the proposed framework by introducing the intensity-range constraint and the base-structure constraint. To preserve details of the input image, the proposed method takes advantage of reconstructing the output image in the gradient domain, while the output intensity is guaranteed to lie within the specified intensity range, e.g. *0-to-255, by the intensity-range constraint. In addition, the reconstructed image lies close to the base structure by the base-structure constraint, which is effective for restraining artifacts. Experimental results show that the proposed framework is effective for various applications such as tone mapping, seamless image cloning, detail enhancement, and image restoration.*

1. Introduction

Natural scenes include base structures and detailed textures of various kinds. Combinations of the base structures and the detailed textures provide rich information. An image editing algorithm, or image filtering, by manipulating the base structures and/or the detailed textures has a crucially important role in computer graphics and computer vision. The applications of such image editing algorithms include seamless image cloning [27], tone mapping for a high-dynamic range image (HDR tone mapping) [12], and detail enhancement [10]. Image editing algorithms for these applications are classifiable as i) gradient-domain approach or ii) layer-decomposition approach.

In the gradient-domain approach [5, 12, 27, 29], the gradients extracted from the input image are manipulated depending on the gradient norm. Roughly speaking, large and small gradients respectively associate to the base structure and the detailed texture. In the HDR tone mapping application [12], for example, large gradients are compressed, while preserving the small gradients. After these gradient manipulations, the gradient-based HDR tone mapping applications integrate the gradients to generate the resultant tone-mapped image. However, the intensity range of the tone-mapped image remains unknown until the integration is performed. Therefore, the intensity range of the tone-mapped image often exceeds a fixed target range, 0-to-255 in general. Image range adjustment such as intensity rescaling or clipping is required as post-processing to enforce the intensity range into 0-to-255. This post-processing generates artifacts such as oversaturation and oversmoothing.

In the layer-decomposition approach [10, 26, 39, 38], the input image is decomposed into the base structure and the detailed texture. Then, the base structure and the detailed texture are manipulated separately. In a detail enhancement application [10], for example, the detailed texture is enhanced and added to the base structure. The base structure should be extracted precisely and carefully to avoid artifacts such as ringing, halos, and gradient reversal. Various sophisticated edge-preserving filters [10, 26, 39, 38] have been proposed to extract the base structure precisely. However, the precise base structure extraction is still a challenging problem.

In this paper, we propose a unified gradient-domain image reconstruction framework that involves gradient-domain and layer-decomposition approaches. The proposed algorithm is an optimization approach based on the target gradient, which incorporates the intensity-range and the base-structure constraints. The proposed algorithm needs no post-processing of the intensity range adjustment because the fixed target intensity range is already taken into account in the optimization with the range constraint. In addition, the base structure constraint proposed in this paper are very effective for restraining artifacts such as ringing and halos.

2. Related works

2.1. Gradient-domain approach

The gradient-domain approach presents various applications for computer graphics and computer vision. For example, the gradient-domain based tone mapping algorithm was proposed by Fattal *et al*. [12]. Perez *et al*. [27] presented the gradient-domain interpolation framework called Poisson image editing. Image fusion techniques based on the gradient-domain were also proposed [29, 9, 35]. Other applications using gradient-domain include image matting [33], inpainting [31, 34], image stitching [22], surface reconstruction [19, 1], color interpolation [21], and color-to-gray mapping [14, 13]. Recently, motivated by the effectiveness of the gradient-domain approach, the general frameworks [5, 17] were also proposed.

The image-processing pipeline of the gradient-domain approach is presented in Fig. 1 (a). The pipeline is mainly composed of three steps: 1) gradient extraction, 2) gradient manipulation, and 3) integration. In existing methods, the intensity range of the integrated image is unknown. Therefore, the intensity range of the reconstructed image often exceeds the fixed target range, *e.g*. 0-to-255, which is the range of a widely used 8-bit image. Intensity-range adjustment such as intensity clipping or rescaling is performed implicitly as post-processing. However, this post-processing of the intensity range adjustment can considerably collapses the gradient information.

2.2. Layer-decomposition approach

The layer-decomposition approach is also widely used for various computer graphics and compute vision applications such as HDR tone mapping [3, 10, 26], image abstraction and image enhancement [10, 26], tone management [4], digital photography [28], and haze removal [30].

The processing pipeline of this approach is shown in Fig. 1 (b). In the layer-decomposition approach, the input image is decomposed into the base structure and the detailed texture. Then, the base structure and/or the detailed texture are manipulated and combined to generate the output image.

In the layer-decomposition, the base structure is first extracted. Then, the detailed texture is obtained by subtracting the base structure from the input image. An edge-preserving filter is usually used to extract the base structure. A well-known edge-preserving filter is the bilateral filter (BLF) [36]. Recently, many researchers have proposed sophisticated edge-preserving filters including the weighted least squares (WLS) filter [10], the guided filter [15], the local Laplacian filters (LLF) [26] and its improved version [2], the bilateral texture filter [6], L_0 smoothing [23, 38], the rolling guidance filter [40], the relative total variation [39], the edge-avoided wavelets [11], the smoothed local histogram filter [18], and the mutual structure for joint filtering [32].

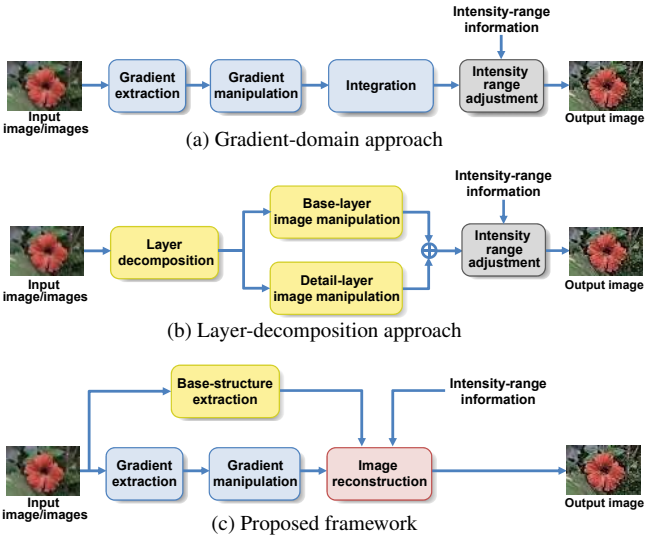

Figure 1. Image processing pipelines of the existing approaches and the proposed framework.

In this approach, the precise base structure extraction is crucially important for the image quality of the output image. Although the recent edge-preserving filtering dramatically improves the performance of the base structure extraction, subtle extraction errors still induces severe artifacts such as halos, ringing, and gradient reversal. Furthermore, similar to the gradient-domain approach, the intensity-range adjustment might be necessary as post-processing.

3. Proposed method

We propose the gradient-domain image reconstruction framework that involves the gradient-domain and layer-decomposition approaches. The pipeline of the proposed method is shown in Fig. 1 (c). The key of the proposed method is the gradient-based reconstruction, which takes account of the intensity-range constraint and the base-structure constraint.

The proposed method first extracts the gradient and the base structure from input images. The gradient contains rich information, whereas the base structure represents the semantically meaningful structure. Next, the gradient is manipulated for each application, as presented in Sec. 4. The final output is reconstructed directly using energy optimization. In the proposed method, in contrast to the existing gradient-domain approach, the base structure and the intensity-range information are used to construct constraints in the energy functional.

3.1. Image reconstruction by optimization

Image reconstruction is performed by optimizing the energy functional, which consists of three terms: 1) the gradient fidelity term, 2) the intensity-range constraint term, and

3) the base-structure constraint term. Formally, the total energy functional $E[u(\mathbf{x})]$ is given as

$$E[u(\mathbf{x})] = F[u(\mathbf{x})] + G_R[u(\mathbf{x})] + G_B[u(\mathbf{x})], \quad (1)$$

where $u(\mathbf{x})$ denotes the output image intensity at the position $\mathbf{x}$, $F[u(\mathbf{x})]$ is the gradient fidelity term, $G_R[u(\mathbf{x})]$ is the intensity-range constraint term, and $G_B[u(\mathbf{x})]$ is the base-structure constraint term.

The target gradient can be preserved in the reconstructed image by minimizing the gradient residual between the target and the reconstructed gradients, in the same manner as the existing gradient-domain approach. The intensity range of the reconstructed image is guaranteed to be within the fixed target range by the intensity-range constraint. The base-structure constraint penalizes if the reconstructed image intensity is far from the base structure, so that the reconstructed image lies close to the base structure.

In this paper, we use a weighted least square of the gradient residuals as the fidelity term, following the method described in Baht *et al*. [5]. The gradient fidelity term can be formulated as

$$F[u(\mathbf{x})] = \int \sum_{d=h,v} w_d(\mathbf{x}) \left|\partial_d u(\mathbf{x}) - q_d(\mathbf{x})\right|^2 d\mathbf{x}, \quad (2)$$

where d stands for the horizontal or the vertical direction, $w_d(\mathbf{x})$ denotes the weight to control the influence of the residual on the result, ∂_d is the partial derivative for each direction, and $q_d(\mathbf{x})$ is the target gradient of each direction. The weight $w_d(\mathbf{x})$ is given as

$$w_d(\mathbf{x}) = \left(\left|\partial_d u_I(\mathbf{x}) - q_d(\mathbf{x})\right| + 1\right)^{-b}, \quad (3)$$

where $u_I(\mathbf{x})$ is the input image intensity at $\mathbf{x}$ and b (typically 0.5 to 8.0) determines the sensitivity to the gradient residual. In the proposed method, $q_d(\mathbf{x})$ is designed for each applications.

The intensity-range constraint term $G_R[u(\mathbf{x})]$ is given formally by integrating the intensity-range constraint $g_R(u(\mathbf{x}))$ over the position $\mathbf{x}$ as

$$G_R[u(\mathbf{x})] = \int g_R(u(\mathbf{x}))d\mathbf{x}, \quad (4)$$

where the intensity-range constraint $g_R(u(\mathbf{x}))$ is defined with infinite potential as

$$g_R(u(\mathbf{x})) = \begin{cases} \infty, & R_{\min} > u(\mathbf{x}) \\ 0, & R_{\min} \le u(\mathbf{x}) \le R_{\max} \\ \infty, & u(\mathbf{x}) > R_{\max}, \end{cases} \quad (5)$$

where $R_{\max}$ and $R_{\min}$ is the upper and lower bound defined by a fixed target range.

Image reconstruction using the two terms above, *i.e*., $F[u(\mathbf{x})]$ and $G_R[u(\mathbf{x})]$, is simple but effective for many applications such as the seamless image cloning and HDR tone mapping applications, as presented in Sec. 4 . Furthermore, by introducing the base-structure constraint term $G_B[u(\mathbf{x})]$, the proposed method can find more extensive applications.

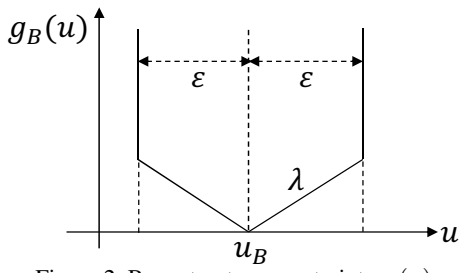

Figure 2. Base structure constraint $g_B(u)$.

3.2. Base structure constraint

The base-structure constraint term $G_B[u(\mathbf{x})]$ is given by integrating the base-structure constraint $g_B(u(\mathbf{x}))$ over the position $\mathbf{x}$ as

$$G_B[u(\mathbf{x})] = \int g_B(u(\mathbf{x}))d\mathbf{x}. \quad (6)$$

In general, artifacts such as ringing and gradient reversal are generated when the output image intensity is excessively separated from the base structure. To penalize the intensity separation, the use of a simple constraint such as least squares form can be considered. This simple constraint can suppress the intensity separation, but it tends to over-smooth the details because the least squares is too strong to preserve the details.

We design the base-structure constraint, so that the intensity separation is suppressed while preserving the details. The proposed base-structure constraint is given as

$$g_B(u(\mathbf{x})) = \begin{cases} \lambda(\mathbf{x})\left|u(\mathbf{x}) - u_B(\mathbf{x})\right|, & \left|u(\mathbf{x}) - u_B(\mathbf{x})\right| \le \varepsilon(\mathbf{x}) \\ \infty, & \left|u(\mathbf{x}) - u_B(\mathbf{x})\right| > \varepsilon(\mathbf{x}), \end{cases} \quad (7)$$

where $u_B(\mathbf{x})$ is the base structure, $\varepsilon(\mathbf{x})$ is the range parameter to decide the target range from the base structure $u_B(\mathbf{x})$, and $\lambda(\mathbf{x})$ is the slope parameter to control the strength of the weak penalty. The base-structure constraint in Eq. (7) represents the convex potential as presented in Fig. 2. This base-structure constraint guarantees that the pixel intensity is within the range $\varepsilon(\mathbf{x})$ from the base structure by the infinity potential. Within the range of $\varepsilon(\mathbf{x})$, the base-structure constraint weakly penalizes the difference between the intensity and the base structure, so that detailed information is preserved. In this paper, we set that $\lambda(\mathbf{x})$ is proportional to the inverse of the square of differences between the input image $u_I(\mathbf{x})$ and the base structure $u_B(\mathbf{x})$.

3.3. Parameter designs of base-structure constraint

By designing the base structure $u_B(\mathbf{x})$ and the range parameter $\varepsilon(\mathbf{x})$, the proposed framework can be applied to various applications such as detail enhancement and im-

age restoration. We present examples of the base structure $u_B(\mathbf{x})$ and the range parameter $\varepsilon(\mathbf{x})$.

Edge-preserving filter based (EPF-based): The standard choice to extract the base structure is applying the edge-preserving filter:

$$u_B(\mathbf{x}) = J(u_I(\mathbf{x})), \qquad \varepsilon(\mathbf{x}) = \varepsilon_0, \tag{8}$$

where $J(\cdot)$ is an edge-preserving filtering, and ε_0 (typically 15 to 45) is the globally constant parameter to determine the target range from the base structure. For example, the design in Eq. (8) is effective for detail enhancement applications.

Local intensity distribution based (LIB-based): In the image restoration application such as non-blind deconvolution, the overshoot or undershoot around edges generates the ringing artifacts. The proposed framework is effective to restrain these artifacts by designing the spatially adaptive range parameter $\varepsilon(\mathbf{x})$. In general, the over or under shooting pixel intensity is prominently larger or smaller than the pixel intensity of its neighbors. To restrain the artifact, the base structure $u_B(\mathbf{x})$ and the range parameter $\varepsilon(\mathbf{x})$ are designed so that the output image intensity $u(\mathbf{x})$ does not exceed the local maximum or minimum of the input image intensity $u_I(\mathbf{x})$ at position $\mathbf{x}$. The base structure and the range parameter can be expressed as

$$\begin{aligned} u_B(\mathbf{x}) &= \frac{1}{2}\Big[\max_{\tilde{\mathbf{x}}\in\mathcal{N}(\mathbf{x})} u_I(\tilde{\mathbf{x}}) + \min_{\tilde{\mathbf{x}}\in\mathcal{N}(\mathbf{x})} u_I(\tilde{\mathbf{x}})\Big], \\ \varepsilon(\mathbf{x}) &= \frac{1}{2}\Big[\max_{\tilde{\mathbf{x}}\in\mathcal{N}(\mathbf{x})} u_I(\tilde{\mathbf{x}}) - \min_{\tilde{\mathbf{x}}\in\mathcal{N}(\mathbf{x})} u_I(\tilde{\mathbf{x}})\Big], \end{aligned} \tag{9}$$

where $\mathcal{N}$ (typically 3 to 7) is the set of neighbor pixel positions around $\mathbf{x}$.

3.4. Analysis of proposed constraints

We demonstrate the advantages of the intensity-range constraint term $G_R[u(\mathbf{x})]$ and the base-structure constraint term $G_B[u(\mathbf{x})]$ using the 1D signal examples.

Fig. 3 (a) shows the 1D signal example. We used the gradient fidelity term $F[u(\mathbf{x})]$ and the intensity-range constraint term $G_R[u(\mathbf{x})]$. Here, the black line shows the input 1D signal. The dotted red lines show the lower and upper bounds, *i.e.*, $R_{\min}$ and $R_{\max}$. In this example, the target gradient $q_d(u(\mathbf{x}))$ is given as $q_d(u(\mathbf{x})) = \partial_d u_I(\mathbf{x})$ for simplicity. The gradient of the input signal is shown in Fig. 3 (b). The weak gradients originated from the details exist between the prominent gradients originated from the strong edges. The close-up of the results obtained using the naive intensity-range adjustment (the clipping and the rescaling), the proposed method and their gradient are shown in Figs. 3 (c)–3 (h).

As shown in Figs. 3 (c) and 3 (d), the over-saturated artifacts are generated by the clipping, whereas the signal is oversmoothed and the detail gradient collapses by rescaling, as shown in Figs. 3 (e) and 3 (f). However, Figs. 3 (g) and 3 (h) show the following: 1) the proposed method can preserve the detail gradient, which collapses by the naive range adjustment; and 2) the range of the obtained signal is within the fixed target range.

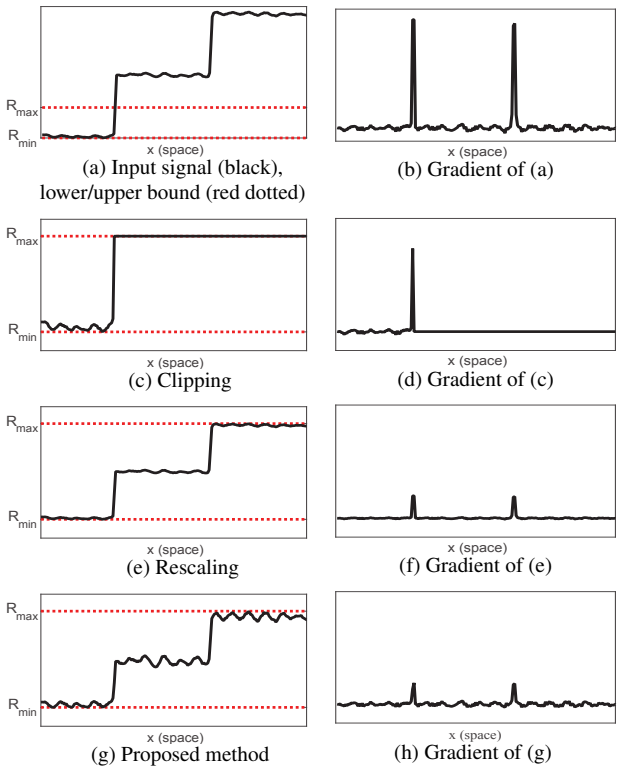

Figure 3. Effectiveness of intensity range constraint $G_R[u(\mathbf{x})]$.

Next, we demonstrate the effectiveness of the base-structure constraint term $G_B[u(\mathbf{x})]$ using 1D signal example shown in Fig. 4. The goal in this example is to restore the blurred signal using the inaccurate (target) gradient $q_d(u(\mathbf{x}))$, which includes over or under shoot. This situation is common in practical scenes because the inaccurate gradient is often obtained when we restore the blurred image using inaccurate blur kernel. Estimating the strictly accurate blur kernel is extremely challenging. In this example, the inaccurate target gradient is calculated based on the image deblurred by existing non-blind deconvolution algorithm with inaccurate blur kernel. The base-structure constraint is calculated using Eq. (9). In Fig 4 (b), the red line shows the base structure $u_B(\mathbf{x})$, whereas the red dotted lines show the lower and upper bounds, *i.e.* $u_B(\mathbf{x}) \pm \varepsilon(\mathbf{x})$.

Results shown by the existing non-blind deconvolution method [20] using the inaccurate blur kernel and the proposed method are shown respectively in Figs. 4 (c) and (d) (black line). Although the existing method can recover sharpness around the strong edge, the ringing artifacts are generated. However, the proposed constraint can restrain the artifacts while maintaining sharpness around the strong edge because the base-structure constraint guarantees that

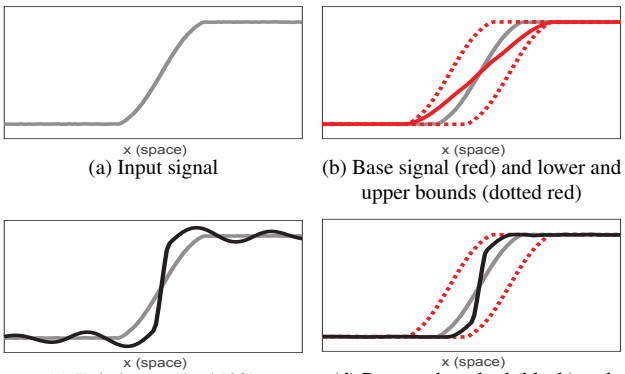

(a) Input signal (b) Base signal (red) and lower and upper bounds (dotted red)

(c) Existing method [20] (d) Proposed method (black) and lower and upper bounds (dotted red)

Figure 4. Effectiveness of base-structure constraint $G_B[u(\mathbf{x})]$.

the restored intensity is within the (spatially-adaptive) target range shown as the red dotted lines.

3.5. Solver by proximal algorithm

The objective functional $E[u(\mathbf{x})]$ is composed of the differential convex term $F[u(\mathbf{x})]$ and the non-differential convex term $G_R[u(\mathbf{x})]$ and $G_B[u(\mathbf{x})]$. The objective functional is convex, but non-differential. Therefore, its solution cannot be obtained in a trivial manner. Fortunately, recent significant progress in convex optimization techniques presents a simple but efficient algorithmic solution. Particularly, the proximal algorithms [8, 25] are a powerful optimization scheme for image processing [24] and computational photography [16]. If there is inexpensive proximal mapping of the non-differential convex terms, *i.e.* $G_R[u(\mathbf{x})]$ and $G_B[u(\mathbf{x})]$, the proximal algorithms can effectively optimize the energy $E[u(\mathbf{x})]$. The proximal algorithms ensure the convergence and the uniqueness of the solution [8, 25]. To minimize the objective functional $E[u(\mathbf{x})]$, we use the proximal algorithms [8, 25]. The proximal algorithm iteratively updates $u(\mathbf{x})$ as

$$u^{k+1}(\mathbf{x}) = \mathrm{prox}_{\eta G}\big(z^k(\mathbf{x})\big), \tag{10}$$

where $\mathrm{prox}_{\eta \mathrm{g}}(\cdot)$ is proximal mapping with step parameter η, G is the non-differential term $G{=}G_R{+}G_B$, $z^k(\mathbf{x})$ is the result obtained by standard gradient descent iteration for the deferential term $F[u(\mathbf{x})]$ which is given by

$$z^k(\mathbf{x}) = u^k(\mathbf{x}) - \eta \frac{\delta F[u(\mathbf{x})]}{\delta u(\mathbf{x})}, \tag{11}$$

where $\delta F[u(\mathbf{x})]/\delta u(\mathbf{x})$ is the functional derivative of $F[u(\mathbf{x})]$. Here, we set $\eta = 0.25$ in this paper. It is noteworthy that the initial value $u^{k=1}$ is given by preprocessing, which is designed for each application. From Eq. (2), the functional derivative of $F[u(\mathbf{x})]$ is described as

$$\frac{\delta F[u(\mathbf{x})]}{\delta u(\mathbf{x})} = -\sum_{d=h,v} \partial_d\big(w_d(\mathbf{x})\,(\partial_d u(\mathbf{x}) - q_d)\big). \tag{12}$$

In our energy, the proximal mapping $\mathrm{prox}_{\eta \mathrm{G}}(\cdot)$ can be calculated position-by-position. The proximal mapping at the position $\mathbf{x}$ can be derived based on the integrand $g(\mathbf{x}) = g_R(\mathbf{x}){+}g_B(\mathbf{x})$ of $G[u(\mathbf{x})]$. In the following, we discuss the proximal mapping of integrand $g(\mathbf{x})$ at the position $\mathbf{x}$, which is denoted by $\mathrm{prox}_{\eta \mathrm{g}}(\cdot)$. To simplify the expression, we omit the argument $\mathbf{x}$. To calculate the proximal mapping $\mathrm{prox}_{\eta \mathrm{g}}(\cdot)$, we rewrite the sum of the intensity-range constraint $g_R(u)$ and the base-structure constraint $g_B(u)$ as

$$g_R(u) + g_B(u) = \Phi(u) + \iota(u), \tag{13}$$

where $\Phi(u)$ is the slope function given as $\Phi(u) = \lambda|u - u_B|$, $\iota(u)$ is the indicator function given as shown below.

$$\iota(u) = \begin{cases} \infty, & \underline{u} > u \\ 0, & \underline{u} \le u \le \overline{u}, \\ \infty, & u > \overline{u} \end{cases} \tag{14}$$

where $\overline{u} = \min(u_B{+}\varepsilon, R_{\max})$ and $\underline{u} = \max(u_B{-}\varepsilon, R_{\min})$ are upper and lower bounds at position $\mathbf{x}$. As shown in Eq. (13), the proposed constraints, *i.e.* $g_R(u)$ and $g_B(u)$, are formally expressed as the summation of the indicator function $\iota(u)$ and the slope function $\Phi(u)$. The proximal mapping $\mathrm{prox}_{\eta \mathrm{g}}(\cdot)$ is calculable as the proximal mapping of the indicator function $\iota(u)$ and the slope function $\Phi(u)$ as follows:

$$\begin{aligned} \mathrm{prox}_{\eta g}(z) &= \mathrm{prox}_{\eta\iota + \eta\Phi}(z) \\ &= \mathrm{prox}_{\eta\iota}\big(\mathrm{prox}_{\eta\Phi}(z)\big) \\ &= P_{[\underline{u},\overline{u}]}\Big(\mathrm{soft}_{[\eta\lambda,\eta\lambda]}\Big(z - u_B\Big) + u_B\Big), \end{aligned} \tag{15}$$

where $P_{[\underline{u},\overline{u}]}(\cdot)$ is the hard thresholding operator by $\underline{u}$ and $\overline{u}$, and $\mathrm{soft}_{[\gamma,\gamma]}(\cdot)$ is the soft thresholding operator by γ [25]. The step parameter η is updated for each step. Consequently, our algorithm for minimizing the energy functional in Eq. (1) can be expressed with simple implementation using the proximal gradient method. The computational cost is proportional to the number of the iteration, and it takes several minutes with non-optimized implementation in matlab.

4. Applications

The proposed framework has various applications including seamless image cloning, HDR tone mapping, image enhancement, image fusion, and image restoration. In this section, we demonstrate the examples of the performance of the proposed framework for each application[1]. The intensity-range constraint and the base-structure constraint for each application are listed in Table 1. The luminance component is reconstructed by the proposed framework. The color component extracted from the input image

[1]The additional results and the source code will be available at http://www.ok.ctrl.titech.ac.jp/res/IC/

Table 1. Examples of intensity-range constraint and base-structure constraint for each application.

Application	$G_R[u(\mathbf{x})]$	$G_B[u(\mathbf{x})]$
Seamless image cloning	✓	-
Tone mapping	✓	-
Detail enhancement	✓	EPF-based
Non-blind deconvolution	✓	LID-based

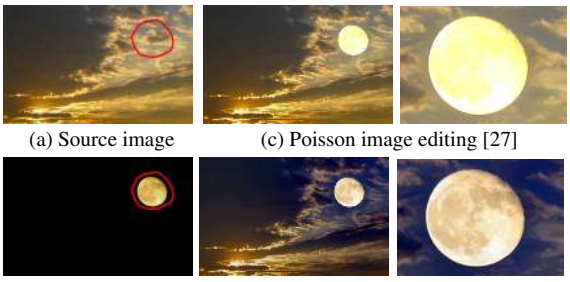

(a) Source image (c) Poisson image editing [27]

(b) Target image (d) Proposed method

Figure 5. Seamless image cloning.

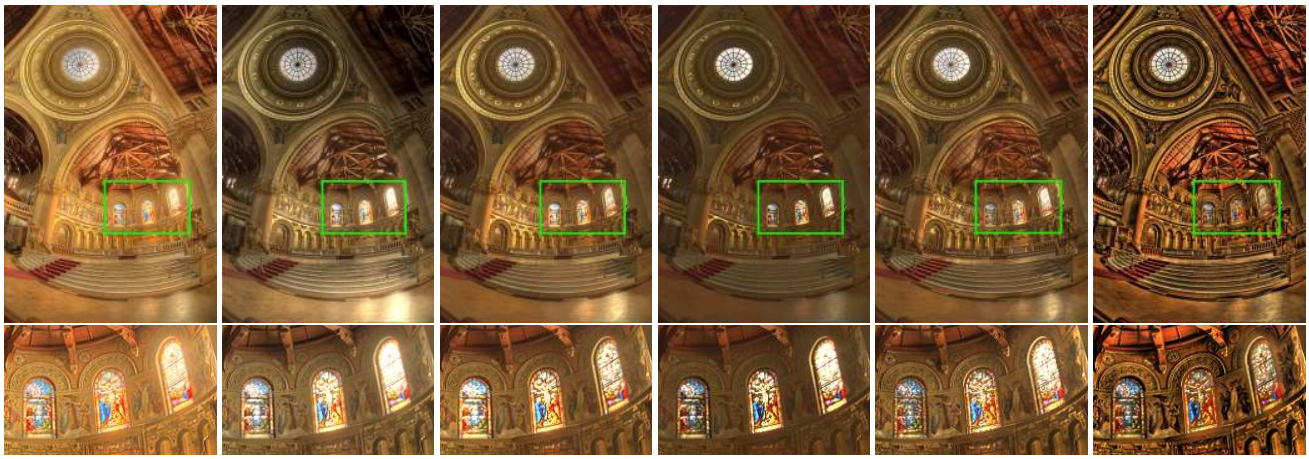

(a) Fattal's method [12] (b) Gradient shop [5] (c) LLF[26] (d) WLS [10] (e) L_0 smoothing [38] (f) Proposed method

Figure 6. HDR tone mapping result.

is added to the reconstructed luminance component.

4.1. Seamless image cloning

The proposed framework is effective for gradient-based image editing applications such as the seamless image cloning. In general, existing methods including Poisson image editing [27] suffer from over-saturation because the intensity range of the integrated image is unknown until the gradient integration is performed. The intensity range after gradient integration often exceeds the fixed target range. On the other hand, the proposed framework using the intensity-range constraint can generate the output within the fixed target range while preserving the details. In this application, the target (combined) gradient $q_d(\mathbf{x})$ is given as $q_d(\mathbf{x}) = \phi(\mathbf{x})\partial_d u_I(\mathbf{x}) + (1-\phi(\mathbf{x}))\partial_d u_T(\mathbf{x})$, where $u_I(\mathbf{x})$ is the source image, $u_T(\mathbf{x})$ is the target image, and $\phi(\mathbf{x})$ is the binary mask which is specified by the user. The initial value $u^{k=1}(\mathbf{x})$ is given by the naive composed intensity as $u^{k=1}(\mathbf{x}) = \phi(\mathbf{x})u_I(\mathbf{x}) + (1-\phi(\mathbf{x}))u_T(\mathbf{x})$.

The results obtained using the proposed and the existing methods [27] are shown respectively in Figs. 5 (c) and 5 (d). Although the detailed texture of the moon are diminished in the result obtained using the existing method [27], as shown in Fig. 5 (c), the proposed method can preserve the detailed texture of the moon, as shown in Fig. 5 (d). It is noteworthy that the proposed method automatically adjusts the whole image intensity to preserve the details under the intensity-range constraint, while the existing method only adjusts the intensity within the specified target region.

4.2. HDR Tone mapping

Our framework with the intensity-range constraint is also effective for the HDR tone mapping application. In this application, the target gradient $q_d(\mathbf{x})$ is given as $q_d(\mathbf{x}) = \alpha\partial_d\tilde{u}_I(\mathbf{x})$, where α is the parameter to control the target gradient strength, $\tilde{u}$ is the normalized input image intensity by dividing by the local maximum of the input image $u_I(\mathbf{x})$. The initial value $u^{k=1}(\mathbf{x})$ is obtained by the naive range adjustment, *i.e.* the intensity rescaling.

An example of the results obtained using the proposed method is shown in Figs. 6 (f) . Here, $\alpha = 0.015$ in this experiment. Comparison with the existing gradient-domain approaches (Fattal *et al.* [12] and Gradient shop [5]), and the existing layer-decomposition approaches (L_0 smoothing [38], Local Laplacian filter (LLF) [26], and WLS filter [10]) are also shown in Figs. 6 (a)–6 (e)[2]. As shown in Fig. 6, the proposed method can generate detail-preserving output without oversaturation in the stained glass region, while the pixel intensity is saturated in the region using ex-

[2]Here, the default setting or the suggested parameters were used for the method [5, 10]. The results by the existing methods [12, 26, 38] are collected by their project pages.

(a) Input image (intensity rescaling) (b) Default setting by the proposed method ($\alpha = 0.015$) (c) Enhanced details by the proposed method ($\alpha = 0.03$)

Figure 7. HDR tone mapping with detail enhancement by adjusting the target gradient strength α in the proposed method.

Table 2. Root mean squared error of gradient components.

Method	Q_G	Method	Q_G
Clipping	11.0	Gradient shop [5]	0.038
Rescaling	0.042	LLF [26]	0.038
Proposed method	**0.027**	WLS [10]	0.040

isting methods.

Another example is shown in Fig. 7. The proposed method can control details by adjusting the target gradient strength α. As shown in Fig. 7 (c), the details of the floor are enhanced by increasing α without saturation.

Finally, to evaluate the performance of our framework, we measured the gradient preservation of the details using root mean squared error of the gradient Q_G:

$$Q_G = \sqrt{\int \sum_{d=h,v} \left|\partial_d u(\mathbf{x}) - q_d(\mathbf{x})\right|^2 d\mathbf{x}}. \qquad (16)$$

In this evaluation, 35 HDR images were used to evaluate the metric Q_G. The average value of the metric of the proposed method and the existing methods are presented in Table 2. Evaluation shows that the proposed method can preserve the details of the gradient better than the existing tone mapping algorithms.

4.3. Detail enhancement

Next, we demonstrate the performance of the proposed method for the detail enhancement application. Using our base-structure constraint term, the proposed method can generate the detail-enhanced image without artifacts such as gradient reversals even though the target gradient is designed simply. To examine this benefit, the simplest design of the target gradient $q_d(\mathbf{x})$ is used as follows: $q_d(\mathbf{x}) = \alpha\partial_d u_I(\mathbf{x})$, where α is the parameter to control the target gradient strength. The input intensity is used as initial value $u^{k=1}(\mathbf{x})$.

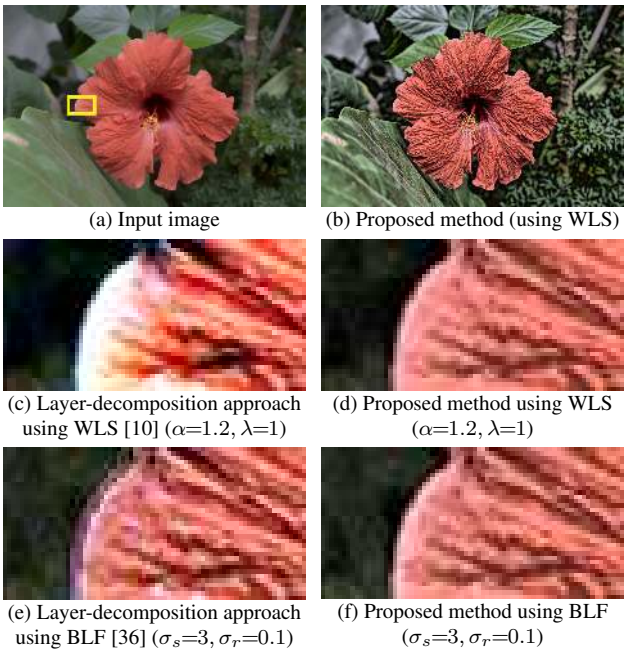

(a) Input image (b) Proposed method (using WLS) (c) Layer-decomposition approach using WLS [10] (α=1.2, λ=1) (d) Proposed method using WLS (α=1.2, λ=1) (e) Layer-decomposition approach using BLF [36] (σ_s=3, σ_r=0.1) (f) Proposed method using BLF (σ_s=3, σ_r=0.1)

Figure 8. Detail enhancement result by the proposed method.

To compare the performance of the proposed method with those of the existing methods based on layer-decomposition approach, we compare the detail enhanced results obtained using the existing methods and the proposed method with the same edge-preserving filter as shown in Fig. 8. Here, we set α=8.0 in this experiment. Using the existing method, gradient reversal and oversaturated artifacts are generated at the edge region, as shown in Figs. 8 (c) and 8 (e). In the results of the existing methods, the artifacts severely appear because the gradient strength factor is relatively large. However, even in this extreme case, the proposed method can restrain the artifacts though the same edge-preserving filter is used to extract the base structure, as shown in Figs. 8 (d) and 8 (f). Furthermore, one can find that the proposed method can generate similar outputs irrespective of the edge-preserving filter algorithms. These results demonstrate that the proposed method is robust against choosing edge-preserving filter algorithms and their parameters.

4.4. Robust restoration: non-blind deconvolution

As discussed in Sec. 3.4, the proposed method with the base-structure constraint term can restore the blurred image using the inaccurate gradient without ringing artifacts. This benefit is considerably effective for non-blind deconvolution with an inaccurate blur kernel. We evaluated the performance of the proposed method for the non-blind

(a) Input image (b) Krishnan's method [20] (c) Cho's method [7] (d) Proposed method (e) Ground truth

Figure 10. Comparison of the proposed method with existing methods.

deconvolution application. It is noteworthy that although the non-blind deconvolution application is discussed in this section, the proposed method is also effective for blind-deconvolution application because, in general, non-blind deconvolution and the blur kernel estimation are alternatively conducted in many blind-deconvolution algorithms.

In this application, the inaccurate (targeted) gradient $q_d(\mathbf{x})$ is calculated based on the image deblurred by an existing non-blind deconvolution algorithm with inaccurate blur kernel. Formally, the inaccurate gradient is given as $q_d(\mathbf{x})=\partial_d\tilde{v}(\mathbf{x})$, where $\tilde{v}(\mathbf{x})$ is the result obtained using the existing non-blind deconvolution method. In this paper, we used Cho's method [7] to obtain $\tilde{v}(\mathbf{x})$.

The blurred image and the result by the proposed method are shown in Fig. 9. A comparison of the proposed method with the existing methods (Krishnan et. al [20] and that of Cho *et al*. [7]) at the blue and the red box regions is shown in Fig. 10. Here, default setting parameters were used for each existing methods. The input image is blurred using the spacially variant kernel based on the depth of each object. The restored images are generated by debluring with the spacially invariant kernel which is for the back ground. As shown in Figs. 10 (b) and 10 (c), the existing methods generate severe ringing artifact in the foreground, *e.g*. the cow, where the image is restored by the inaccurate blur kernel. The proposed method can dramatically reduce the ringing artifact while maintaining the sharpness of the strong edge in the background where the image is restored by the accurate blur kernel.

To evaluate the robustness against the blur kernel inaccuracy, we conducted the experiment using kernels having different kernel width. The true width of the setting kernel is $\sigma=2$ [pix]. The Peak Signal-to-Noise Ratio (PSNR) and SSIM [37] between the ground truth and the restored results are presented in Fig. 11. These figures show that the proposed method outperforms the existing methods in terms of both measures when the kernel width σ is greater than the true width, because the existing methods generate strong ringing artifacts, while the proposed method can restrain it. This result shows that the proposed method is effective for

(a) Input image (b) Result by Proposed method

Figure 9. Results of non-blind deconvolution.

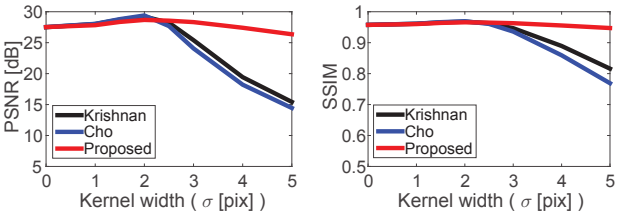

(a) PSNR (b) SSIM

Figure 11. Robustness against inaccurate blur kernels.

robust image restoration using the inaccurate gradient such as non-blind deconvolution application with the inaccurate blur kernel.

5. Conclusions

We have proposed the novel gradient-domain image reconstruction framework with the intensity-range constraint and the base-structure constraint. The intensity-range constraint can generate an image with intensity within the fixed target range. By introducing the base-structure constraint, the proposed method can generate detail-preserving output while reducing artifacts. The proposed framework can inherit the benefit of the existing gradient-domain approach and the layer-decomposition approach. Experiments have shown that the proposed framework has various applications such as tone mapping, seamless image cloning, detail enhancement, and image restoration.

References

[1] A. Agrawal, R. Chellappa, and R. Raskar. An algebraic approach to surface reconstruction from gradient fields. *Proc. of IEEE Int. Conf. on Computer Vision(ICCV)*, 1:174–181, 2005.

[2] M. Aubry, S. Paris, S. W. Hasinoff, J. Kautz, and F. Durand. Fast local laplacian filters: Theory and applications. *ACM Trans. on Graphics (TOG)*, 33(5):167, 2014.

[3] T. O. Aydin, N. Stefanoski, S. Croci, M. Gross, and A. Smolic. Temporally coherent local tone mapping of hdr video. *ACM Trans. on Graphics (TOG)*, 33(6):196, 2014.

[4] S. Bae, S. Paris, and F. Durand. Two-scale tone management for photographic look. *ACM Transactions on Graphics (TOG)*, 25(3):637–645, 2006.

[5] P. Bhat, C. L. Zitnick, M. Cohen, and B. Curless. Gradientshop: A gradient-domain optimization framework for image and video filtering. *ACM Trans. on Graphics (TOG)*, 29(2):10, 2010.

[6] H. Cho, H. Lee, H. Kang, and S. Lee. Bilateral texture filtering. *ACM Trans. on Graphics (TOG)*, 33(4):128, 2014.

[7] S. Cho, J. Wang, and S. Lee. Handling outliers in non-blind image deconvolution. *Proc. of IEEE Int. Conf. on Computer Vision(ICCV)*, pages 495–502, 2011.

[8] P. L. Combettes and J. C. Pesquet. Proximal splitting methods in signal processing. *Fixed-point algorithms for inverse problems in science and engineering*, pages 185–212, 2011.

[9] D. Connah, M. S. Drew, and G. D. Finlayson. Spectral edge image fusion: Theory and applications. *Proc. of European Conf. on Computer Vision (ECCV)*, pages 65–80, 2014.

[10] Z. Farbman, R. Fattal, D. Lischinski, and R. Szeliski. Edge-preserving decompositions for multi-scale tone and detail manipulation. *ACM Trans. on Graphics (TOG)*, 27(3):67, 2008.

[11] R. Fattal. Edge-avoiding wavelets and their applications. *ACM Trans. on Graphics (TOG)*, 28(3):22, 2009.

[12] R. Fattal, D. Lischinski, and M. Werman. Gradient domain high dynamic range compression. *ACM Trans. on Graphics (TOG)*, 21(3):249–256, 2002.

[13] G. D. Finlayson, D. Connah, and M. S. Drew. Lookup-table-based gradient field reconstruction. *IEEE Trans. on Image Processing*, 20(10):2827–2836, 2011.

[14] A. A. Gooch, S. C. Olsen, J. Tumblin, and B. Gooch. Color2gray: salience-preserving color removal. *ACM Trans. on Graphics (TOG)*, 24(3):634–639, 2005.

[15] K. He, J. Sun, and X. Tang. Guided image filtering. *Proc. of European Conf. on Computer Vision (ECCV)*, 6311:1–14, 2010.

[16] F. Heide, M. Steinberger, Y. T. Tsai, M. Rouf, D. Pajak, D. Reddy, O. Gallo, J. Liu, W. Heidrich, K. Egiazarian, et al. Flexisp: A flexible camera image processing framework. *ACM Trans. on Graphics (TOG)*, 33(6):231, 2014.

[17] M. Hua, X. Bie, M. Zhang, and W. Wang. Edge-aware gradient domain optimization framework for image filtering by local propagation. *Proc. of the Conf. on Computer Vision and Pattern Recognition (CVPR)*, pages 2838–2845, 2014.

[18] M. Kass and J. Solomon. Smoothed local histogram filters. *ACM Trans. on Graphics (TOG)*, 29(4):100, 2010.

[19] M. Kazhdan, M. Bolitho, and H. Hoppe. Poisson surface reconstruction. *Proc. of the fourth Eurographics symposium on Geometry processing*, 7, 2006.

[20] D. Krishnan and R. Fergus. Fast image deconvolution using hyper-laplacian priors. *Advances in Neural Information Processing Systems (NIPS)*, pages 1033–1041, 2009.

[21] A. Levin, D. Lischinski, and Y. Weiss. Colorization using optimization. *ACM Trans. on Graphics (TOG)*, 23(3):689–694, 2004.

[22] A. Levin, A. Zomet, S. Peleg, and Y. Weiss. Seamless image stitching in the gradient domain. *Proc. of European Conf. on Computer Vision (ECCV)*, pages 377–389, 2004.

[23] R. Nguyen and M. S. Brown. Fast and effective L0 gradient minimization by region fusion. *Proc. of IEEE Int. Conf. on Computer Vision(ICCV)*, 2015.

[24] S. Ono and I. Yamada. A convex regularizer for reducing color artifact in color image recovery. *Proc. of the Conf. on Computer Vision and Pattern Recognition (CVPR)*, pages 1775–1781, 2013.

[25] N. Parikh and S. Boyd. Proximal algorithms. *Foundations and Trends in optimization*, 1(3):123–231, 2013.

[26] S. Paris, S. W. Hasinoff, and J. Kautz. Local laplacian filters: edge-aware image processing with a laplacian pyramid. *ACM Trans. on Graphics (TOG)*, 30(4):68, 2011.

[27] P. Pérez, M. Gangnet, and A. Blake. Poisson image editing. *ACM Trans. on Graphics (TOG)*, 22(3):313–318, 2003.

[28] G. Petschnigg, R. Szeliski, M. Agrawala, M. Cohen, H. Hoppe, and K. Toyama. Digital photography with flash and no-flash image pairs. *ACM Trans. on Graphics (TOG)*, 23(3):664–672, 2004.

[29] R. Raskar, A. Ilie, and J. Yu. Image fusion for context enhancement and video surrealism. *Proc. of Int. Symp. on Non-Photorealistic Animation and Rendering (NPAR)*, (7):85 – 152, 2004.

[30] L. Schaul, C. Fredembach, and S. Süsstrunk. Color image dehazing using the near-infrared. *Proc. of IEEE Int. Conf. on Image Processing (ICIP)*, 2009.

[31] J. Shen, X. Jin, C. Zhou, and C. C. Wang. Gradient based image completion by solving the poisson equation. *Computers & Graphics*, 31(1):119–126, 2007.

[32] X. Shen, C. Zhou, L. Xu, and J. Jia. Mutual-structure for joint filtering. *Proc. of IEEE Int. Conf. on Computer Vision(ICCV)*, 2015.

[33] J. Sun, J. Jia, C. K. Tang, and H. Y. Shum. Poisson matting. *ACM Trans. on Graphics (ToG)*, 23(3):315–321, 2004.

[34] J. Sun, L. Yuan, J. Jia, and H. Y. Shum. Image completion with structure propagation. *ACM Trans. on Graphics (ToG)*, 24(3):861–868, 2005.

[35] J. Sun, H. Zhu, Z. Xu, and C. Han. Poisson image fusion based on markov random field fusion model. *Information Fusion*, 14(3):241–254, 2013.

[36] C. Tomasi and R. Manduchi. Bilateral filtering for gray and color images. *Proc. of IEEE Int. Conf. on Computer Vision(ICCV)*, pages 839–846, 1998.

[37] Z. Wang, A. C. Bovik, H. R. Sheikh, and E. P. Simoncelli. Image quality assessment: from error visibility to structural similarity. *IEEE Trans. on Image Processing*, 13(4):600–612, 2004.

[38] L. Xu, C. Lu, Y. Xu, and J. Jia. Image smoothing via L 0 gradient minimization. *ACM Trans. on Graphics (TOG)*, 30(6):174, 2011.

[39] L. Xu, Q. Yan, Y. Xia, and J. Jia. Structure extraction from texture via relative total variation. *ACM Trans. on Graphics (TOG)*, 31(6):139, 2012.

[40] Q. Zhang, X. Shen, L. Xu, and J. Jia. Rolling guidance filter. *Proc. of European Conf. on Computer Vision (ECCV)*, pages 815–830, 2014.